

Hyperentangled mixed phased Dicke states: optical design and detection

A. Chiuri,¹ G. Vallone,^{2,1} N. Bruno,¹ C. Macchiavello,³ D. Bruß,⁴ and P. Mataloni^{1,5}

¹*Dipartimento di Fisica, Sapienza Università di Roma, I-00185 Roma, Italy*

²*Museo Storico della Fisica e Centro Studi e Ricerche Enrico Fermi,*

Via Panisperna 89/A, Compendio del Viminale, I-00184 Roma, Italy

³*Dipartimento di Fisica “A. Volta” and INFN-Sezione di Pavia, via Bassi 6, 27100 Pavia, Italy*

⁴*Institut für Theoretische Physik III, Heinrich-Heine-Universität Düsseldorf, D-40225 Düsseldorf, Germany*

⁵*Istituto Nazionale di Ottica Applicata (INO-CNR), L.go E. Fermi 6, I-50125 Firenze, Italy*

(Dated: September 27, 2018)

We present an experimental method to produce 4-qubit phased Dicke states, based on a source of 2-photon hyperentangled states. By introducing quantum noise in the multipartite system in a controlled way, we have tested the robustness of these states. To this purpose the entanglement of the resulting multipartite entangled mixed states has been verified by using a new kind of structural witness.

The generation and detection of multipartite entangled states is a remarkable challenge that needs to be accomplished in order to fully explore and exploit the genuine quantum features of quantum information and many-body physics. So far only a limited number of families of pure multipartite entangled states has been experimentally produced. In view of future applications, it is particularly important to test the robustness of the generated states in the presence of unavoidable noise coming from the environment. Here, we produce a new family of multipartite maximally entangled states, we experimentally introduce certain types of noise in a controlled way and test the robustness properties of the states.

The experimental generation of multipartite entangled states that we propose is based on hyperentangled photons [1], which allows to produce symmetric and phased Dicke states. Dicke states have recently attracted much interest, and have been produced in experiments with photons [2–4]. Phased Dicke states represent a more general family of entangled states with respect to the ordinary symmetric Dicke states: they are achieved by introducing phase changes starting from ordinary Dicke states.

In order to test the presence of multipartite entanglement we may adopt different kinds of entanglement witnesses. Their experimental implementations are presented, e.g., in Refs. [5] for bipartite qubits, and [2–4, 6] for pure symmetric multipartite states. In this work we implement a recently proposed new class of entanglement witnesses, so-called structural witnesses [7], and further extend such a class in order to achieve higher efficiency in entanglement detection. Moreover, we test the robustness of the phased Dicke states by introducing dephasing noise in a controlled fashion and provide a measurement of the lower bound on the robustness of entanglement. In this way we provide a new experimental tool to investigate the entanglement properties of multipartite mixed states.

An entanglement witness is defined as a Hermitian operator W that detects the entanglement of a state

ρ if it has a negative expectation value for this state, $\langle W \rangle_\rho = \text{Tr}(\rho W) < 0$ while at the same time $\text{Tr}(\sigma W) \geq 0$ for all separable states σ [8, 9]. For a composite system of N particles, the structural witnesses [7] have the form

$$W(k) := \mathbb{1}_N - \Sigma(k), \quad (1)$$

where k is a real parameter (the wave-vector transfer in a scattering scenario), $\mathbb{1}_N$ is the identity operator and

$$\Sigma(k) = \frac{1}{2}[\bar{\Sigma}(k) + \bar{\Sigma}(-k)] \quad (2)$$

with

$$\begin{aligned} \bar{\Sigma}(k) &= \frac{1}{B(N,2)} \left(c_x \hat{S}^{xx}(k) + c_y \hat{S}^{yy}(k) + c_z \hat{S}^{zz}(k) \right), \\ c_i &\in \mathbb{R}, |c_i| \leq 1. \end{aligned} \quad (3)$$

Here $B(N, 2)$ is the binomial coefficient and the structure factor operators $\hat{S}^{\alpha\beta}(k)$ are defined as

$$\hat{S}^{\alpha\beta}(k) := \sum_{i < j} e^{ik(r_i - r_j)} S_i^\alpha S_j^\beta, \quad (4)$$

where i, j denote the i -th and j -th spins, r_i, r_j their positions in a one-dimensional scenario, and S_i^α are the spin operators with $\alpha, \beta = x, y, z$. In the following we normalize the distances with the labels of the qubits as $r_i - r_j = i - j$. In the present work we focus on the case of 4-qubits phased Dicke states defined as [7]:

$$\begin{aligned} |D_4^{ph}\rangle &= \frac{1}{\sqrt{6}} (|0011\rangle + |1100\rangle + |0110\rangle + |1001\rangle \\ &\quad - |0101\rangle - |1010\rangle). \end{aligned} \quad (5)$$

A suitable structural witness for the above phased Dicke state is given by the operator (1) with $k = \pi$, $c_x = c_y = c_z = 1$ and S_i^α being the Pauli operators [7]. This witness leads to $\text{Tr}(|D_4^{ph}\rangle \langle D_4^{ph}| W) = -\frac{4}{9}$.

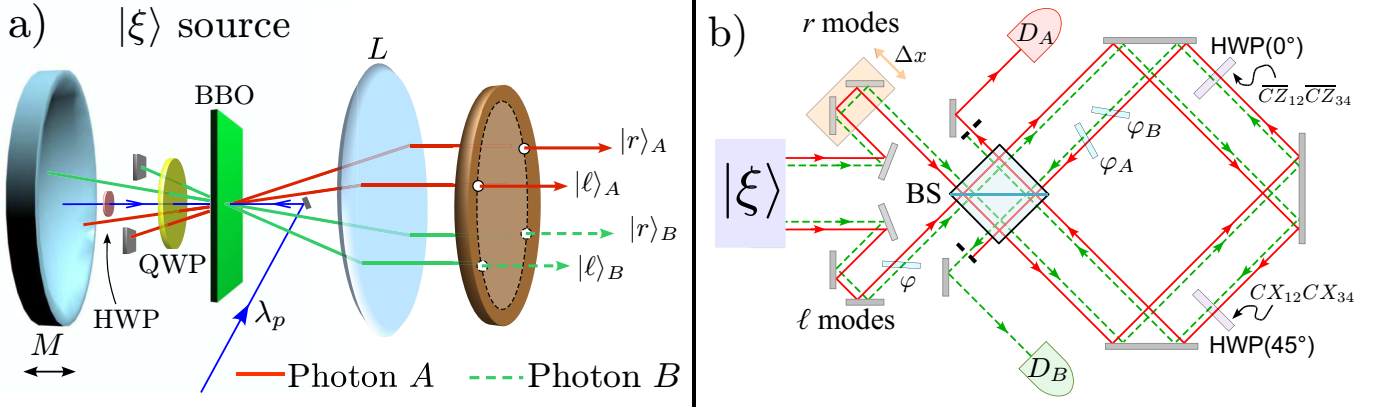


FIG. 1: Generation of the 4-qubit phased Dicke state. a) Scheme of the entangled 2-photon 2-qubit parametric source that generates the state $|\xi\rangle$. Mirror M reflects both the UV pump beam and the parametric radiation. The lens L is used to obtain parallel modes at the output of the 4-hole screen. HWP (QWP) is an half- (quarter-) waveplate. b) Optical setup used to transform $|\xi\rangle$ into the state $|D_4^{(ph)}\rangle$ and to measure Pauli operators. The phase φ is used to properly generate $|\xi\rangle$ while φ_A and φ_B are used to measure Pauli momentum operators for the A and B photon respectively.

A wider class of structural witness can be obtained by generalizing the operator given in (3) to linear superpositions of structure factor operators $\hat{S}^{\alpha\beta}(k)$ evaluated for different values of k :

$$\bar{\Sigma}(k^x, k^y, k^z) = \frac{1}{B(N,2)} \left(c_x \hat{S}^{xx}(k^x) + c_y \hat{S}^{yy}(k^y) + c_z \hat{S}^{zz}(k^z) \right) \quad (6)$$

$$c_i \in \mathbb{R}, |c_i| \leq 1.$$

Following the same argument as in [7], it can be shown that any operator of the form (6) combined as in (1) has non-negative expectation values for separable states and is therefore an entanglement witness. Using this more general construction for the present experiment we consider a witness operator with $k^x = k^y = \pi$ and $k^z = 0$:

$$\bar{W} = \mathbb{1}_N - \frac{1}{6} \left(\hat{S}^{xx}(\pi) + \hat{S}^{yy}(\pi) - \hat{S}^{zz}(0) \right). \quad (7)$$

The expectation value of the above witness for the phase Dicke state (5) is given by $\text{Tr}(|D_4^{ph}\rangle\langle D_4^{ph}| \bar{W}) = -\frac{2}{3}$.

State generation - We will now describe the method to generate phased Dicke states and to implement controlled noise, and present the experimental results of entanglement detection. Let's consider the following state $|\xi\rangle \equiv \frac{1}{\sqrt{6}}(|0010\rangle - |1000\rangle + 2|0111\rangle)$. It is easy to show that the phased Dicke state can be obtained by applying a unitary transformation¹ \mathcal{U} to the state $|\xi\rangle$:

$$|D_4^{(ph)}\rangle = Z_4 \overline{CZ}_{12} \overline{CZ}_{34} CX_{12} CX_{34} H_1 H_3 |\xi\rangle \equiv \mathcal{U} |\xi\rangle \quad (8)$$

where H_j and Z_j stands for the Hadamard and the Pauli σ_z transformations on qubit j , $CX_{ij} = |0\rangle_i \langle 0| \mathbb{1}_j +$

$|1\rangle_i \langle 1| X_j$ is the controlled-NOT gate and $\overline{CZ}_{ij} = |1\rangle_i \langle 1| \mathbb{1}_j + |0\rangle_i \langle 0| Z_j$ the controlled-Z. We realized the Dicke state by using 4-qubits encoded into polarization and path of two parametric photons [A and B in figure 1a)]. The $|0\rangle$ and $|1\rangle$ states are encoded into horizontal $|H\rangle$ and vertical $|V\rangle$ polarization or into right $|r\rangle$ and left $|\ell\rangle$ path. Explicitly, we used the following correspondence between physical states and logical qubits:

$$\{|0\rangle_1, |1\rangle_1\} \rightarrow \{|r\rangle_A, |\ell\rangle_A\} \quad (9)$$

$$\{|0\rangle_2, |1\rangle_2\} \rightarrow \{|H\rangle_A, |V\rangle_A\} \quad (10)$$

$$\{|0\rangle_3, |1\rangle_3\} \rightarrow \{|r\rangle_B, |\ell\rangle_B\} \quad (11)$$

$$\{|0\rangle_4, |1\rangle_4\} \rightarrow \{|H\rangle_B, |V\rangle_B\} \quad (12)$$

According to these relations the state $|\xi\rangle$ reads:

$$|\xi\rangle = \frac{1}{\sqrt{6}} [|HH\rangle (|r\ell\rangle - |\ell r\rangle) + 2|VV\rangle |r\ell\rangle] \quad (13)$$

and may be obtained by suitably modifying the source used to realize polarization-momentum hyperentangled states [1, 10]. In each “ket” of (13) the first (second) term refers to particle A (B). A vertically polarized UV laser beam impinges on a Type I β -barium borate (BBO) nonlinear crystal in two opposite directions, back and forth, and determines the generation of the polarization entangled state corresponding to the superposition of the spontaneous parametric down conversion (SPDC) emission at degenerate wavelength [see Fig. 1a)]. A 4-hole mask selects four optical modes (two for each photon), namely $|r\rangle_A$, $|\ell\rangle_A$, $|r\rangle_B$ and $|\ell\rangle_B$, within the emission cone of the crystal. The SPDC contribution, due to the pump beam incoming after reflection on mirror M , corresponds to the term $|HH\rangle (|r\ell\rangle - |\ell r\rangle)$, whose weight is determined by a half waveplate intercepting the UV beam (see [11] for more details on the generation of the

¹ An equivalent and more simple transformation is given by $\mathcal{U} = Z_1 CX_{12} CX_{34} H_1 H_3$. We used the transformation given in (8) in order to compensate the optical delay introduced by the CX gates in the Sagnac loop of Fig. 1b).

non-maximally polarization entangled state). The other SPDC contribution $2|VV\rangle|r\ell\rangle$ is determined by the first excitation of the pump beam: here the $|\ell r\rangle$ modes are intercepted by two beam stops and a quarter waveplate QWP transforms the $|HH\rangle$ SPDC emission into $|VV\rangle$ after reflection on mirror M . The relative phase between the $|VV\rangle$ and $|HH\rangle$ is varied by translation of the spherical mirror.

The transformation (8) $|\xi\rangle \rightarrow |D_4^{(ph)}\rangle$ is realized by using waveplates and one beam splitter (BS): the two Hadamards H_1 and H_3 in (8), acting on both path qubits, are implemented by a single BS for both A and B modes. For each controlled-NOT (or controlled-Z) gate appearing in (8) the control and target qubit are respectively represented by the path and the polarization of a single photon: a half waveplate (HWP) with axis oriented at 45° (0°) with respect to the vertical direction and located into the left $|\ell\rangle$ (right $|r\rangle$) mode implements a CX (CZ) gate.

After these transformations, the optical modes are spatially matched for a second time on the BS, closing in this way a “displaced Sagnac loop” interferometer that allows high stability in the path Pauli operator measurements [see Fig. 1b)]. Polarization Pauli operators are measured by standard polarization analysis setup in front of detectors D_A and D_B (not shown in the figure). Note that, the $|0\rangle$ ($|1\rangle$) states are identified by the counterclockwise (clockwise) modes in the Sagnac loop.

Decoherence - We will now describe how we introduced a controlled decoherence into the system (we mention that recently controlled decoherence has been implemented in an ion trap experiment [12]). Consider a single photon in a Mach-Zehnder interferometer with two arms (left and right). Varying the relative delay $\Delta x = \ell - r$ between the right and left arm corresponds to a single qubit path decoherence channel given by $\rho \rightarrow (1-p)\rho + pZ\rho Z$. The parameter p is related to Δx : when $\Delta x > \tau$, where τ represents the photon coherence time, then $p = \frac{1}{2}$, while when $\Delta x = 0$ we have $p = 0$. This can be understood by observing that there are two time bins (one for each path). By varying the optical delay, we entangle the path with the time bin degree of freedom (DOF). Hence, by tracing over time we obtain decoherence in the path DOF depending on the overlap between the two time bins. In our setup, this can be obtained by changing the relative delay $\Delta x = \ell - r$ between the right and the left modes of the photons in the first interferometer shown in Fig. 1. Since the translation stage acts simultaneously on both photons, this operation corresponds to two path decoherence channels:

$$\rho \rightarrow (1-q_2)^2\rho + q_2(1-q_2)[Z_1\rho Z_1 + Z_3\rho Z_3] + q_2^2 Z_1 Z_3 \rho Z_1 Z_3 \quad (14)$$

where the parameter q_2 is related to Δx in the following way. Let's consider the path terms in the $|HH\rangle$ contribution in $|\xi\rangle$, namely $|\psi^-\rangle = \frac{1}{\sqrt{2}}(|r\ell\rangle - |\ell r\rangle)$.

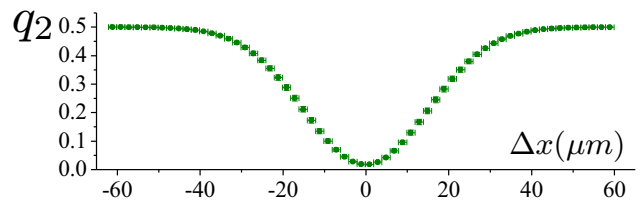


FIG. 2: Values of q_2 corresponding to different values of the path delay Δx .

The decoherence acts by (partially) spoiling the coherence between the $|r\ell\rangle$ and $|\ell r\rangle$ term giving the state $\frac{1}{2}(|\ell r\rangle\langle\ell r| + |r\ell\rangle\langle r\ell|) - \frac{1}{2}(1 - 2q_2)^2(|\ell r\rangle\langle r\ell| + |r\ell\rangle\langle\ell r|)$. By assuming that for $|\psi^-\rangle$ the decoherence (14) is the main source of imperfections, the measured visibility² $\tilde{V}_{exp}(\Delta x)$ of first interference on BS may be compared with the calculated value $\tilde{V} = (1 - 2q_2)^2$: then, the relation between Δx and q_2 , shown in Fig. 2, is obtained. It is worth noting that at $\Delta x = 0$ we have $q_2 = 0.0175 \pm 0.0001$ which corresponds to a maximum visibility $V_{exp} = 0.9313 \pm 0.0005$ at $\Delta x = 0$.

The decoherence channel (14) acts on the state $|\xi\rangle$. However, it can be interpreted as a decoherence acting on the phased Dicke state $|D_4^{(ph)}\rangle$. Using equation (8) and the relations $\mathcal{U}Z_1\mathcal{U}^\dagger = -Y_1Y_2$ and $\mathcal{U}Z_3\mathcal{U}^\dagger = Y_3Y_4$, the channel (14) may be interpreted as a *collective decoherence channel* on $|D_4^{(ph)}\rangle$:

$$|D_4^{(ph)}\rangle\langle D_4^{(ph)}| \rightarrow \sum_{j=1}^4 B_j |D_4^{(ph)}\rangle\langle D_4^{(ph)}| B_j^\dagger \quad (15)$$

with $B_1 = (1 - q_2)\mathbb{1}$, $B_2 = \sqrt{q_2(1 - q_2)}Y_1Y_2$, $B_3 = \sqrt{q_2(1 - q_2)}Y_3Y_4$ and $B_4 = q_2Y_1Y_2Y_3Y_4$. A collective decoherence is a decoherence process that cannot be seen as the action of several channels acting separately on two (or more) qubits. A different type of collective noise, introduced in [13], was experimentally demonstrated in [14] for two polarization qubits in optical fibers.

Two other main sources of imperfections must be considered in our setup (see supplementary informations for a detailed discussion): the first one is due to a non perfect superposition between forward and backward SPDC emission, i.e. between the $|HH\rangle$ and $|VV\rangle$ contributions. This imperfection can be modeled as a phase polarization decoherence channel acting on qubit 2: $\rho \rightarrow (1 - q_1)\rho + q_1Z_2\rho Z_2$. By selecting in $|\xi\rangle$ the correlated modes $|r\ell\rangle$ and by suitably setting the

² The measured visibility is defined as $\tilde{V}_{exp}(\Delta x) = \frac{B-C}{B}$ where B are the coincidences measured out of interference (i.e. measured for Δx much longer than the single photon coherence length) and C the coincidences measured in a given position of Δx .

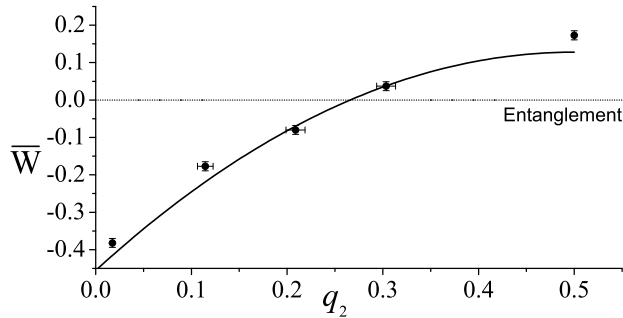


FIG. 3: Experimental values of the witness \overline{W} as a function of q_2 . The dark curve corresponds to the theoretical curve obtained by setting $q_1 = 0.05$ and $q_3 = 0.05$.

HWP on the pump beam we obtain the following state: $\frac{1}{\sqrt{2}}(|HH\rangle_{AB} + e^{i\gamma}|VV\rangle_{AB})|rl\rangle$. Even in this case the value of the measured polarization visibility ($V_\pi \simeq 0.90$) can be related to the polarization decoherence channel as $q_1 = \frac{1-V_\pi}{2} \simeq 0.05$. The second interference on the BS (i.e. after the Sagnac loop) has been also investigated. In the measurement condition we obtained an average visibility of $V_{k_2} \simeq 0.80$ corresponding to a decoherence channel $\rho \rightarrow (1 - q_3)^2 \rho + q_3(1 - q_3)[Z_1 \rho Z_1 + Z_3 \rho Z_3] + q_3^2 Z_1 Z_3 \rho Z_1 Z_3$ with $q_3 = 0.05$.

Measurements - We measured the witness operator (7) for different values of q_2 . The results are shown in figure 3. The dark curve corresponds to the theoretical curve obtained by considering all the three described decoherence channels and setting $q_1 = 0.05$ and $q_3 = 0.05$ (see the supplementary informations about the details on the theoretical curve). Notice that the noise parameter for which the witness expectation value vanishes gives a lower bound on the robustness of the entanglement of the produced state with respect to the implemented noise. The witness \overline{W} measured for the phased Dicke state is

$$\langle \overline{W} \rangle_{exp} = -0.382 \pm 0.012 \quad (16)$$

We also measured a witness W_{mult} introduced in [15] to demonstrate that the generated state $|D_4^{(ph)}\rangle$ is a genuine multipartite state and to obtain a bound on the fidelity F . Its expression is given in the supplementary informations. We obtained

$$\langle W_{mult} \rangle = -0.341 \pm 0.015 \quad \rightarrow \quad F \geq 0.780 \pm 0.005 \quad (17)$$

Following the approach of quantitative entanglement witnesses [16], we can also use the experimental result on the expectation value of the witness to provide a lower bound on the *random robustness* of entanglement E_r . This is defined in [17] to be the maximum amount of

white noise that one can add to a given state ρ before it becomes separable. A lower bound on $E_r(\rho)$ is given by

$$E_r(\rho) \geq \frac{D|\text{Tr}(\rho \overline{W})|}{\text{Tr}(\overline{W})}, \quad (18)$$

where D is the dimension of the Hilbert space on which ρ acts. In our experiment the witness from Eq. (7) and its expectation value given in Eq. (16) lead to

$$E_r(\rho) \geq |\langle \overline{W} \rangle_{exp}| = 0.382 \pm 0.012 \quad (19)$$

In summary, we have generated phased 4-qubit Dicke states with hyperentangled photons. We demonstrated the implementation of controlled noise via a relative path delay in the interferometer. The multipartite entanglement was detected via a new class of structural entanglement witnesses and the robustness of entanglement was tested by using an intrinsically high phase stability setup. The realized phase Dicke states have a high fidelity and, compared with other Dicke states based on 4-photon entanglement, are produced at higher repetition rate.

This work was supported in part by the EU projects CORNER, DFG project and by Finanziamento Ateneo 2009 of Sapienza Università di Roma.

-
- [1] M. Barbieri, C. Cinelli, P. Mataloni, and F. De Martini, Phys. Rev. A **72**, 052110 (2005).
 - [2] N. Kiesel, C. Schmid, G. Tóth, E. Solano, and H. Weinfurter, Phys. Rev. Lett. **98**, 063604 (2007).
 - [3] R. Prevedel, G. Cronenberg, M. S. Tame, M. Paternostro, P. Walther, M. S. Kim, and A. Zeilinger, Phys. Rev. Lett. **103**, 020503 (2009).
 - [4] W. Wieczorek, R. Krischek, N. Kiesel, P. Michelberger, G. Tóth, and H. Weinfurter, Phys. Rev. Lett. **103**, 020504 (2009).
 - [5] M. Barbieri, F. De Martini, G. Di Nepi, P. Mataloni, G. M. D'Ariano, and C. Macchiavello, Phys. Rev. Lett. **91**, 227901 (2003).
 - [6] M. Bourennane, M. Eibl, C. Kurtsiefer, S. Gaertner, H. Weinfurter, O. Gühne, P. Hyllus, D. Bruß, M. Lewenstein, and A. Sanpera, Phys. Rev. Lett. **92**, 087902 (2004).
 - [7] P. Krammer, H. Kampermann, D. Bruß, R. A. Bertlmann, L. C. Kwek, and C. Macchiavello, Phys. Rev. Lett. **103**, 100502 (2009).
 - [8] M. Horodecki, P. Horodecki, and R. Horodecki, Phys. Lett. A **223**, 1 (1996).
 - [9] B. M. Terhal, Phys. Lett. A **271**, 319 (2000).
 - [10] R. Ceccarelli, G. Vallone, F. De Martini, P. Mataloni, and A. Cabello, Phys. Rev. Lett. **103**, 160401 (2009).
 - [11] G. Vallone, E. Pomarico, F. De Martini, P. Mataloni, and M. Barbieri, Phys. Rev. A **76**, 012319 (2007).
 - [12] J. T. Barreiro, P. Schindler, O. Gühne, T. Monz, M. Chwalla, C. F. Roos, M. Hennrich, and R. Blatt, arXiv:1005.1965.

- [13] C. Macchiavello and G. M. Palma, *Phys. Rev. A* **65**, 050301 (2002).
- [14] K. Banaszek, A. Dragan, W. Wasilewski, and C. Radzewicz, *Phys. Rev. Lett.* **92**, 257901 (2004).
- [15] G. Töth, W. Wieczorek, R. Krischek, N. Kiesel, P. Michelberger, and H. Weinfurter, *New Journal of Physics* **11**, 083002 (2009).
- [16] J. Eisert, F. G. S. L. Brandao, and K. M. R. Audenaert, *New Journal of Physics* **9**, 46 (2007).
- [17] G. Vidal and R. Tarrach, *Phys. Rev. A* **59**, 141 (1999).

SUPPLEMENTARY INFORMATION

Let's now describe in more detail the considered decoherence sources. First of all, in our setup, there is a polarization decoherence at the level of the $|\xi\rangle$ generation due to a non perfect superposition between the $|HH\rangle$ and $|VV\rangle$ emission. Since $|\xi\rangle$ is given by the superposition of $|HH\rangle$ and $|VV\rangle$ terms, our decoherence partially erases the coherence between them but cannot introduce terms containing $|VH\rangle$ or $|HV\rangle$. This decoherence can be modeled by a phase decoherence channel acting on polarization qubit 2:

$$\rho \rightarrow (1 - q_1)\rho + q_1 Z_2 \rho Z_2 \quad (20)$$

By exploiting the same arguments used to obtain (15), the channel (20) can be interpreted as a decoherence channel on $|D_4^{(ph)}\rangle$. Since $\mathcal{U}Z_2\mathcal{U}^\dagger = Z_1Z_2$, the polarization decoherence (20) can be written as

$$|D_4^{(ph)}\rangle\langle D_4^{(ph)}| \rightarrow \sum_{j=1}^2 A_j |D_4^{(ph)}\rangle\langle D_4^{(ph)}| A_j^\dagger \quad (21)$$

with $A_1 = \sqrt{1 - q_1}\mathbb{1}$ and $A_2 = \sqrt{q_1}Z_1Z_2$. By measuring the visibility of polarization interference we estimated $q_1 \simeq 0.05$.

The second decoherence affects the path degree of freedom and corresponds to the channel given in eq. (14). We can change the parameter q_2 by varying the delay Δx in the first interferometer. In figure 2 we show the relation between the parameter q_2 and the path delay Δx .

A third decoherence effect, again in the path degree of freedom, is related to the second interference on the BS. The non-perfect interference can be modeled as a decoherence channel acting exactly as (14). Written in the Kraus representation it reads:

$$|D_4^{(ph)}\rangle\langle D_4^{(ph)}| \rightarrow \sum_{k=1}^4 C_k |D_4^{(ph)}\rangle\langle D_4^{(ph)}| C_k^\dagger \quad (22)$$

with $C_1 = (1 - q_3)\mathbb{1}$, $C_2 = \sqrt{q_3(1 - q_3)}Z_1$, $C_3 = \sqrt{q_3(1 - q_3)}Z_3$ and $C_4 = q_3Z_1Z_3$. By measuring the interference visibility we estimated $q_3 \simeq 0.05$.

The three decoherence channels can be summarized as follows

$$\rho(q_1, q_2, q_3) \equiv \sum_{k=1}^4 \sum_{j=1}^4 \sum_{i=1}^2 C_k B_j A_i |D_4^{(ph)}\rangle\langle D_4^{(ph)}| A_i^\dagger B_j^\dagger C_k^\dagger \quad (23)$$

From the previous expression, it is possible to calculate the theoretical expectation values of the operators appearing in the witness as a function of the q 's parameters: (7):

$$\begin{aligned} \langle S_{xx}(\pi) \rangle &= 4 - \frac{8}{3}q_3(3 - q_3) \\ &\quad - \frac{16}{3}(1 - q_3)^2[q_1(1 - 2q_2)^2 + 2q_2(1 - q_2)] \\ \langle S_{yy}(\pi) \rangle &= 4 - \frac{16}{3}q_1(1 - q_3)^2 + \frac{8}{3}(q_3 - 3)q_3 \\ \langle S_{zz}(0) \rangle &= -2 + \frac{16}{3}q_2(1 - q_2) \end{aligned} \quad (24)$$

For $q_1 = 0.05$ and $q_3 = 0.05$ we obtain the following expectation value for \overline{W} :

$$\langle \overline{W} \rangle = -0.455 + 2.333 q_2 - 2.333 q_2^2 \quad (25)$$

This expression is used for the theoretical curve in figure 3.

The witness used to detect multipartite entanglement (see eq. (36) of [15]) is

$$W_{mult} = \frac{1}{8} [21 - 2S_{xx}(\pi) - 2S_{yy}(\pi) + S_{zz}(0) - 2X_1X_2X_3X_4 - 2Y_1Y_2Y_3Y_4 - 7Z_1Z_2Z_3Z_4] \quad (26)$$

By following [15] it is possible to obtain a bound for the fidelity:

$$F > \frac{2}{3} - \frac{1}{3}\langle W_{mult} \rangle. \quad (27)$$